How to cite: *Angew. Chem. Int. Ed.* **2025**, *64*, e202421137
doi.org/10.1002/anie.202421137

Coordination Cages

Chiral Pd_2L_4 Capsules from Readily Accessible Tröger's Base Ligands Inducing Circular Dichroism on Fullerenes C_{60} and C_{70}

Elie Benchimol[+], Helen M. O'Connor[+], Björn Schmidt, Nicola Bogo, Julian J. Holstein, June I. Lovitt, Sankarasekaran Shanmugaraju, Christopher J. Stein,* Thorfinnur Gunnlaugsson,* and Guido H. Clever**

Abstract: The induction of chirality on pristine fullerenes through non-covalent embedding in an asymmetric nano-confinement has only been rarely reported. Bringing molecules with such a unique electronic structure and broad application range into a chiral environment is particularly appealing for the development of chiroptical materials, enantioselective photoredox catalysts and systems showing chirality-induced spin selectivity (CISS). In this study, we report the formation of a chiral, configurationally stable Pd_2L_4 capsule assembled from a C_2-symmetric, 'ribbon-shaped' ligand with a Tröger's base naphthalimide (TbNaps) backbone, easily synthesized in three steps from commercially available compounds. Embedding chirality directly into the ligand backbone ensures a relatively lightweight receptor design whose aromatic panels create a strongly shielded inner cavity of about 700 Å^3 volume. Fullerenes C_{60} and C_{70}, as well as a pair of corannulenes, can be bound in acetonitrile (where unsubstituted fullerenes are insoluble) and X-ray structures of host-guest complexes were obtained. Tight interactions between the chiral host and the fullerene guests leads to the induction of a circular dichroism (CD) on the characteristic absorption bands of the forbidden π–π* transitions of the fullerenes, backed up by sTDA TD-DFT calculations and detailed investigation of the electronic excited states.

Introduction

Fullerenes are among the most extensively studied molecules in chemistry, renowned not only for their unique spherical structures but also for their distinct electronic properties, leading to broad applications in materials science,[1] photovoltaics,[2] molecular electronics,[3] and medicine.[4] Fullerenes and supramolecular chemistry have been closely intertwined over the years,[5] especially because fullerene purification and selective derivatization are notoriously challenging tasks that have greatly benefited from advancements in the field of weak interactions. Numerous supramolecular hosts have been developed to interact with fullerenes, facilitating their separation, chemical modification and application as materials. These hosts include for example organic rings and cages,[6–10] tweezers,[11,12] metal–organic frameworks (MOFs),[13–15] and discrete coordination-driven architectures.[16–19] Recently, this last category has garnered considerable attention, mostly because of the ease of synthesis and modularity of such compounds, obtained by self-assembly between simple organic building blocks and metal ions in solution.[20,21] Several studies have shown the encapsulation of the most common fullerenes C_{60} or C_{70} but also of bigger ones such as C_{84} or derivatives such as PCBM.[22–30] More recently, there has been a growing interest in developing hosts that control the precise covalent functionalization of fullerenes.[23,31–34] However, one area that remained largely underexplored is the introduction of chirality into such vessels, going along with a transfer of this chirality to the encapsulated fullerene guest. There are only

[*] Dr. E. Benchimol,[+] B. Schmidt, Dr. J. J. Holstein, Prof. Dr. G. H. Clever
Department of Chemistry and Chemical Biology, TU Dortmund University, Otto-Hahn-Straße 6, 44227 Dortmund (Germany)
E-mail: guido.clever@tu-dortmund.de

Dr. H. M. O'Connor,[+] Dr. J. I. Lovitt, Prof. Dr. T. Gunnlaugsson
School of Chemistry, Centre for Synthesis and Chemical Biology and Trinity Biomedical Sciences Institute, Trinity College Dublin, College Green, Dublin 2 (Ireland)
E-mail: helen.oconnor@ucd.ie
gunnlaut@tcd.ie

N. Bogo, Prof. Dr. C. J. Stein
Department of Chemistry and Catalysis Research Center, TUM School of Natural Sciences, Technische Universität München (Germany)
E-mail: christopher.stein@tum.de

Dr. S. Shanmugaraju
Department of Chemistry, Indian Institute of Technology Palakkad, 678623 Kerala (India)

[+] These authors have contributed equally.

a few reports on chiral induction onto fullerenes through supramolecular interactions and most of these focus on fullerene networks featuring extensive guest-guest interactions.[35–39] Tightly closed supramolecular capsules, as compared to their more open-meshed cage analogs, often show intimate host-guest interactions. This has been showcased by Yoshizawa and co-workers in their studies on the encapsulation of a wide variety of neutral guests, including fullerenes, in anthracene-panelled Pd_2L_4 capsules,[40–42] just recently also including a chiral derivative carrying exohedral sugar attachments.[43]

A few years ago, some of us reported dibenzo[2.2.2]-bicyclo-octane- and triptycen-based ribbon-shaped ligands to create lightweight, shielded Pd_2L_4 assemblies that encapsulate various polyaromatic hydrocarbons, including fullerenes.[22,23,44] Others of us studied a range of polycyclic aromatic derivatives of the chiral Tröger's base motif, featuring a similar 'ribbon-shaped' core structure as the aforementioned ligands, for a wide range of applications.[45–47] Recently, we teamed up to combine the design of modularly self-assembled, atom-economic hosts for fullerenes with the inherent chirality of Tröger's base.

While Tröger's bases were first introduced into metallosupramolecular assemblies by the Lützen group,[48–53] we herein report the first chiral Pd_2L_4 coordination capsule obtained from a Tröger's base backbone with naphthalimide (Nap) moieties ensuring an almost fully enclosed cavity. We show it to encapsulate either a pair of corannulenes, a single C_{70} and also selectively extract C_{60} from complex mixtures of polyaromatic hydrocarbons, highlighting its potential for purification applications. Furthermore, we show that the chirality of the host is transferred to the encapsulated fullerene guest as we could observe Cotton effects emerging from the absorption bands of the forbidden $t_{1u}\leftarrow h_u$ fullerene electronic transitions.

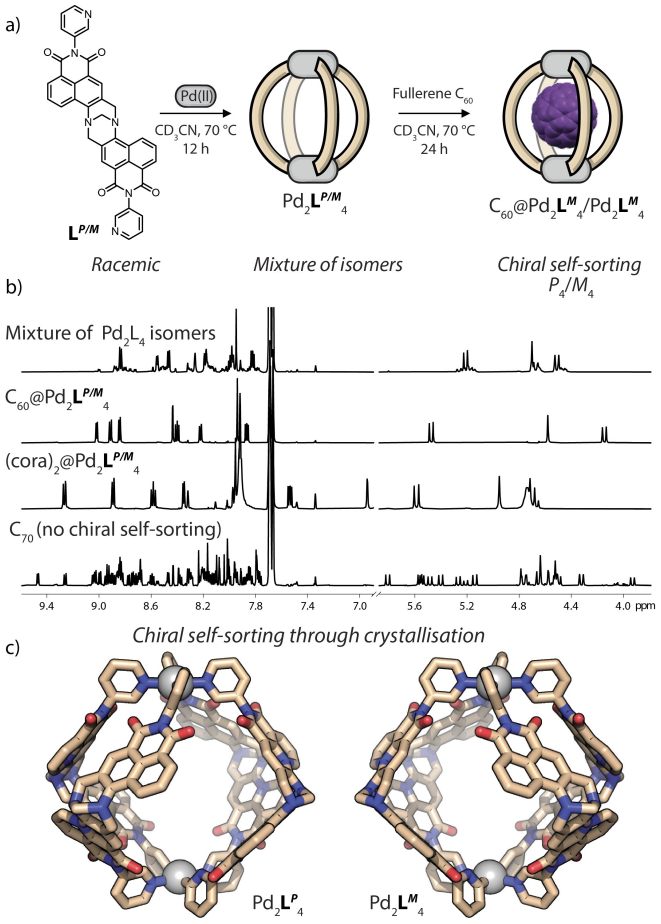

Figure 1. a) Self-assembly of racemic ligand $\mathbf{L}^{P/M}$ with Pd(II) cations. Complete narcissistic chiral self-sorting occurs only upon guest encapsulation. b) Stacked ^{1}H NMR spectra (298 K, CD_3CN, 500 MHz) of the mixture of cage isomers and the outcomes of the encapsulating different PAHs. c) X-ray structures of the two cage enantiomers resulting from chiral self-sorting during crystallization.

Results and Discussion

The 1,8-naphthalimide Tröger's base (**TBNap**) ligand $\mathbf{L}^{P/M}$ used herein was synthesised as its racemate through a modified three-step procedure previously used in the Gunnlaugsson group (SI),[45–47] starting from the commercially available 4-nitro-1,8-naphthalic anhydride and 3-amino-pyridine. Combining racemic $\mathbf{L}^{P/M}$ with a Pd(II) precursor such as $[Pd(CH_3CN)_4](BArF)_2$ (tetrakis[(3,5-trifluoromethyl)phenyl]borate, BArF, as large, non-coordinating counter anion) or $[Pd(CH_3CN)_4](BF_4)_2$ in a 2:1 ratio in DMSO-d_6 or CD_3CN produced one major set of resonances in the ^{1}H NMR spectrum which we attributed to the formation of both of the homochiral $Pd_2\mathbf{L}^{P}{}_4/Pd_2\mathbf{L}^{M}{}_4$ lantern-shaped cages (Figure 1b). However, several other signals could be observed in the spectrum, and we inferred that a smaller number of other isomers were also concomitantly formed. Hence, fully narcissistic chiral self-sorting was not achieved under these conditions. Further evidence for the formation of the dinuclear $Pd_2\mathbf{L}_4$ motif in solution was obtained by ESI-MS analysis (observation of 4+, 3+ and 2+ charged species) and by ^{1}H NMR DOSY spectroscopy (SI). On the other hand, we observed clean narcissistic chiral self-sorting upon crystallisation, and single crystals containing the two enantiomers $Pd_2\mathbf{L}^{P}{}_4/Pd_2\mathbf{L}^{M}{}_4$ in a 1:1 ratio (racemic mixture of the two enantiomers in triclinic space group $P\bar{1}$) could be grown by slow solvent evaporation from a mixture of the $\mathbf{L}^{P/M}$ **TBNap** ligand and $[Pd(CH_3CN)_4](BF_4)_2$ in chloroform/acetonitrile over two weeks. The structure resembles a Pd_2L_4 lantern in which the two Pd^{II} ions are linked by four ligands, providing a Pd–Pd distance of ≈14 Å. Void volume calculations were performed on the $Pd_2\mathbf{L}_4$ skeleton by a rolling probe method using the Molovol software[54] (probe sizes = 2.8 Å, 6 Å), revealing an internal cavity of more than 700 Å^3 (Figure S73). The size and spherical shape of the cavity, along with the tightly arranged aromatic naphthalimide panels, were anticipated to provide an optimal environment for the binding of larger polycyclic aromatic hydrocarbon (PAH) guests.

Indeed, upon heating the mixture of the isomeric $Pd_2\mathbf{L}_4$ assemblies and powdered fullerene C_{60} at 85 °C overnight in CD_3CN (or DMSO-d_6), the colour of the solution was observed to change from yellow to brownish. The ^{1}H NMR

spectrum revealed a single new set of ^{1}H signals, showing downfield shifting for all protons on the naphthalimide units, with the inward-facing protons of the cage (H_a) shifting upfield, indicating an interaction with the π-rich surface of C_{60} (Figure 1b). In the ^{13}C NMR spectrum (CD_3CN), a prominent signal at 141.2 ppm corresponding to encapsulated fullerene C_{60} was also observed. A similar phenomenon occurred when we offered corannulene (cora) as guest, as the mixture converged towards a unique set of signals corresponding to host-guest complex $(cora)_2@Pd_2\mathbf{L}^{P}_4$/$Pd_2\mathbf{L}^{M}_4$ (Figure 1b). Hence, the system underwent complete narcissistic chiral sorting in solution, templated by interaction with the guest molecules. When the cage mixture was stirred at 85 °C in the presence of C_{70}, a similar colour change could be observed, with the sample turning reddish. The ^{1}H NMR spectrum, however, remained very complex and we attribute this to either the formation of several isomers of the host-guest complex in solution (in terms of composition of enantiomeric ligands), or the desymmetrization of the host-guest complexes by conformationally locked, non-spherical C_{70}, or a combination of both (Figure 1b). The exclusive formation of dinuclear cages containing a single fullerene was confirmed by HR-ESI-MS where solely the signal of $[C_{70}@Pd_2\mathbf{L}_4]^{4+}$ was identified (Figure S53).

Next, the two **TBNap** enantiomers were separated by chiral HPLC on an IA Chiralpak column using a mixture of DCM and MeOH (97.5/2.5) as eluent. The ^{1}H NMR spectra in CD_3CN of the two separate fractions were identical to that of the racemic mixture in the same solvent (Figure S15) and showed mirror image behaviour in circular dichroism (CD) spectroscopy. By comparing the signs of the observed Cotton effects with literature values reported for similar derivatives possessing the same **TBNap** core structure, we could empirically assign the absolute configuration.[51] This assignment was further confirmed by X-ray crystallography of the cages formed from the (isolated) enantiomers, using the anomalous diffraction method (Flack parameter 0.028(7) and 0.05(2) for $Pd_2\mathbf{L}^{P}_4$ and $Pd_2\mathbf{L}^{M}_4$ respectively; Figure 1c and Table S3–4). Consequently, the first eluted fraction corresponds to the $\mathbf{L}^{M}$ enantiomer, while the second is attributed to the $\mathbf{L}^{P}$ enantiomer.

When mixed in CD_3CN with a Pd(II) source, enantiomerically pure ligands $\mathbf{L}^{P}$ or $\mathbf{L}^{M}$ yielded the anticipated cages $Pd_2\mathbf{L}^{P}_4$ or $Pd_2\mathbf{L}^{M}_4$ as pure products (from this point forward, we use a single enantiomer notation unless the behaviours of the enantiomeric cages are being compared). The resulting cages displayed a single set of signals in the ^{1}H NMR spectrum, matching the major set of signals of the mixture resulting from the use of the racemic ligand (Figure 2a). The $Pd_2\mathbf{L}_4$ stoichiometry could again be unambiguously confirmed by using ESI-MS analysis, as well as DOSY NMR, which yielded a hydrodynamic radius of $r_h = 12.8$ Å (in CD_3CN) which is typical for this type of dinuclear cage assembly. Finally, as mentioned above, we obtained crystals of both the $Pd_2\mathbf{L}^{P}_4$ and $Pd_2\mathbf{L}^{M}_4$ cages by slow vapor diffusion

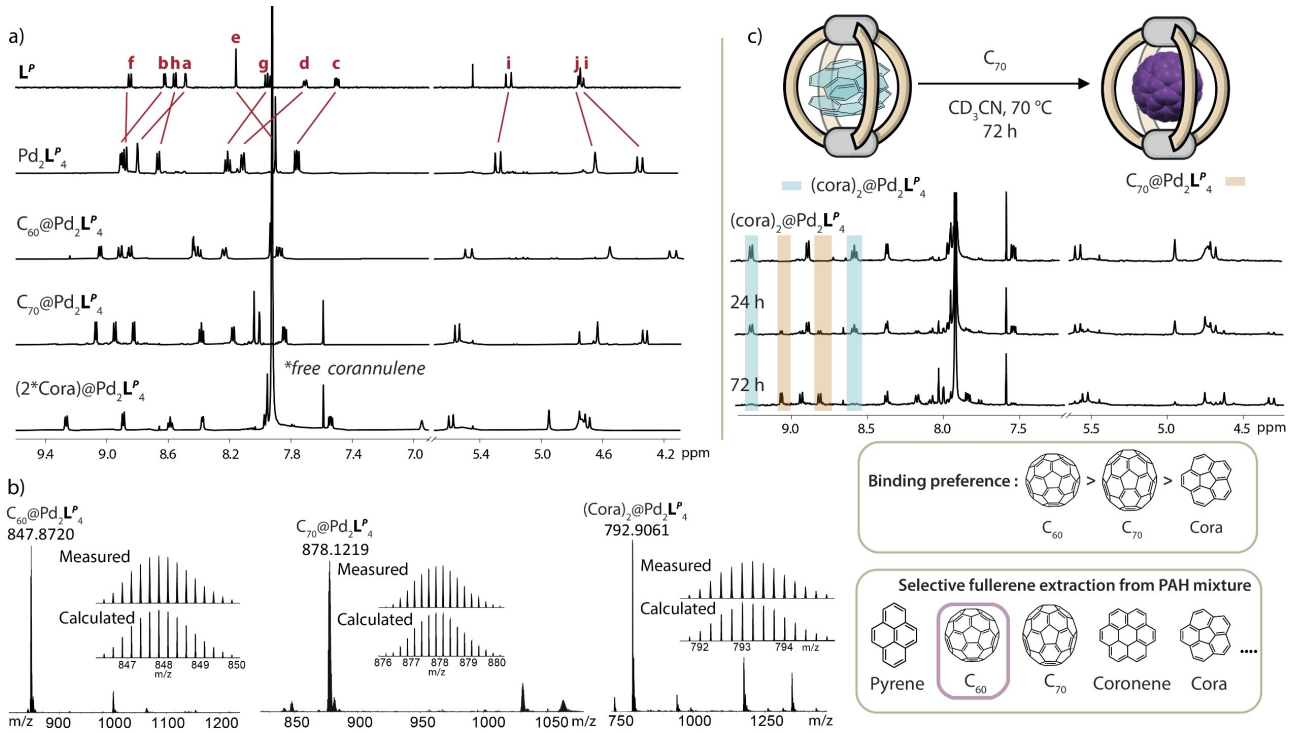

Figure 2. a) Stacked ^{1}H NMR (298 K, CD_3CN, 500 MHz) spectra of enantiopure **TBNap** ligand $\mathbf{L}^{P}$, enantiopure cage $Pd_2\mathbf{L}^{P}_4$ and host-guest complexes $C_{60}@Pd_2\mathbf{L}^{P}_4$, $C_{70}@Pd_2\mathbf{L}^{P}_4$ and $(cora)_2@Pd_2\mathbf{L}^{P}_4$. b) HR-ESI-MS spectra of $C_{60}@Pd_2\mathbf{L}^{P}_4$, $C_{70}@Pd_2\mathbf{L}^{P}_4$ and $(cora)_2@Pd_2\mathbf{L}^{P}_4$. Magnified areas correspond to the 4+ species without counter anion and show the measured and calculated isotopic patterns. c) Corannulene displacement by C_{70} upon heating the sample over 72 hours. The two boxes highlight the binding preferences established through competition experiments as well as the selective fullerene purification from a complex mixture of PAHs.

of diverse solvents into acetonitrile solutions (see Supporting Information for structures).

Next, we examined all ligands and assemblies by UV/Vis absorption spectroscopy. In accordance with a previously reported derivative bearing a para-pyridine donor group,[55] ligand $\mathbf{L}^{PM}$ showed an absorption band in the UV region centred at 346 nm, which corresponds to a π–π* transition, as well as a broader band around 385 nm attributed to an internal charge transfer (ICT) transition of the **TBNap** unit (Figures 4a, S58). Following its coordination to Pd(II) cations, the absorption properties remain nearly identical to those of the free ligand with no significant shifts of these bands, despite slight changes in their absorbance. The addition of a small excess of Pd(II) did not further alter this spectrum, confirming that the fully assembled $Pd_2\mathbf{L}^{M}_4$ cages were the only relevant compounds even at the lower concentrations used for these optical spectroscopy experiments. Additionally, both the ligand and the cage exhibited a shoulder in the far-UV region, clearly observable at 265 nm. The similarities between ligand and cage enantiomers were also reflected in their CD spectroscopic profiles.

We then proceeded to investigate the host-guest properties of the enantiopure assemblies. As with the racemic cage mixture, homochiral cage $Pd_2\mathbf{L}^{P}_4$ could take up one fullerene C_{60} or two molecules of corannulene (Figure 2a). When a solution of the cage was stirred at 70 °C in the presence of an excess of C_{70} powder, the ^{1}H NMR signals of the assembly shifted significantly, with the shift of the inward-pointing proton H_a being notably affected (Figure 2a). These changes in the chemical environment, comparable to observations made for other host-guest systems, indicate the encapsulation of fullerene C_{70} within the available inner space of the cage. The encapsulation of the three guests was further confirmed by ESI-MS analysis, where prominent peaks for $[C_{60}@Pd_2\mathbf{L}^{P}_4]^{4+}$, $[C_{70}@Pd_2\mathbf{L}^{P}_4]^{4+}$ or $[(cora)_2@Pd_2\mathbf{L}^{P}_4]^{4+}$ could be identified in the respective spectra (Figure 2b). We attempted the encapsulation of several other planar aromatic guests (coronene, pyrene, benzopyrene), but these efforts were unsuccessful. As the solubility of fullerene is dramatically low in CD_3CN, we could not directly determine the binding constants for these host-guest interactions in this solvent. However, competition experiments enabled us to establish a ranking of the binding strengths between the three guests as follows: $C_{60} > C_{70} >$ cora. When a preformed solution of $(cora)_2@Pd_2\mathbf{L}^{P}_4$ (still with corannulene excess, as it is slightly soluble in acetonitrile) was stirred at 70 °C in presence of powdered C_{60} or C_{70}, we observed the slow and gradual replacement of corannulene in the cavity (see Figure 2c for example and Figure S54–56). After 72 h, the guest exchange reactions were completed and only the signals corresponding to $C_{60}@Pd_2\mathbf{L}^{P}_4$ (SI) or $C_{70}@Pd_2\mathbf{L}^{P}_4$ (Figure 2c), respectively, could be observed by NMR. On the other hand, when a solution of empty $Pd_2\mathbf{L}^{P}_4$ was stirred at 70 °C in the presence of C_{60} and C_{70} (SI), the recorded ^{1}H NMR spectrum after 24 h showed only signals corresponding to $C_{60}@Pd_2\mathbf{L}^{P}_4$. Further heating did not lead to any changes. Thus, we conclude that this represents the thermodynamic minimum of the system and not a kinetically trapped state. We could also demonstrate the selective extraction and purification of C_{60} from a mixture containing several PAHs (see box in Figure 2), or from carbon soot. When those mixtures were stirred with an acetonitrile solution of $Pd_2\mathbf{L}^{P}_4$, C_{60} was the only PAH taken up by the cage assembly. Following this, addition of toluene and centrifugation resulted in precipitation of the $C_{60}@Pd_2\mathbf{L}^{P}_4$ host-guest complex and solubilization of the other PAHs. We could then recover uniquely the $C_{60}@Pd_2\mathbf{L}^{P}_4$ species (Figure S57).

More intriguingly, when $C_{60}@Pd_2\mathbf{L}^{P}_4$ was stirred in a biphasic system with carbon disulfide (CS_2), no fullerene release was observed, attesting an extremely strong affinity of the cage for the guest, as compared to the reported example of a similar extraction experiment.[22] The replacement of corannulene is most likely driven by both entropy (as one fullerene releases two molecules of corannulene) and enthalpy (with an increase in favourable π–π interactions between the host and guest) effects. On the other hand, we attribute the selective binding of C_{60} over C_{70} to a better fit of spherical C_{60} to the globular cavity of $Pd_2\mathbf{L}^{P}_4$.

These arguments could be confirmed by obtaining crystals of $(cora)_2@Pd_2\mathbf{L}^{P}_4$ and $C_{60}@Pd_2\mathbf{L}^{M}_4$ suitable for synchrotron diffraction analysis, as well as by preparing a DFT-optimized model (ωB97X-D/def2-SVP) for $C_{70}@Pd_2\mathbf{L}^{P}_4$ (Figure 3). The host-guest species $(cora)_2@Pd_2\mathbf{L}^{P}_4$ crystallizes in the *C2* space group while $C_{60}@Pd_2\mathbf{L}^{M}_4$ does so in the *P1* one. Comparing the crystal structure of the empty host with those of the host-guest complexes indicates an induced-fit phenomenon, also referred to as the "breathing" mechanism.[56,57] In the empty cage, the Pd–Pd distance measures 14.0 Å, while the average N–N distance between the oppositely arranged Tröger's base backbone nitrogen atoms is 17.1 Å (Figure 3a), respectively. The same distances in the $C_{60}@Pd_2\mathbf{L}^{P}_4$ host-guest complex are 15.5 Å and 15.3 Å, respectively. In contrast, in the $(cora)_2@Pd_2\mathbf{L}^{P}_4$ complex, they are 14.8 Å and 16.3 Å, respectively. Apparently, the host undergoes a lateral contraction (concomitantly with an increase of the Pd–Pd distance) to maximize the host-guest π–π interactions. Such breathing phenomenon was also observed in the DFT-optimized structures of all the host-guest complexes (Table S1). The perfect fit of fullerene C_{60} within the cavity of $Pd_2\mathbf{L}^{P}_4$ is emphasized by visualizing the Conolly surface representation of the guest that shows a nearly fully occupied inner space (Figure 3b).

These strong interactions between the chiral host and the guests prompted us to investigate the photophysical characterisation of these systems further (Figure 4). Encapsulation of fullerene C_{60} in a 1:1 manner resulted in a clear rise of the far-UV band observed in the absorption spectrum, with the shoulder initially located at 265 nm becoming a clear band centred at the same wavelength (Figure 4a). This effect is also observed for C_{70}, however in a more moderate fashion. The C_{60} binding also leads to a broadening of the following band, previously centred at 346 nm, and concomitantly, two new maxima can be observed around 338 nm and 348 nm, respectively. Eventually, the band centred at 385 nm undergoes a hypsochromic effect, as well as a more pronounced tailing observable up to 500 nm at this concentration. While C_{70} leads to similar

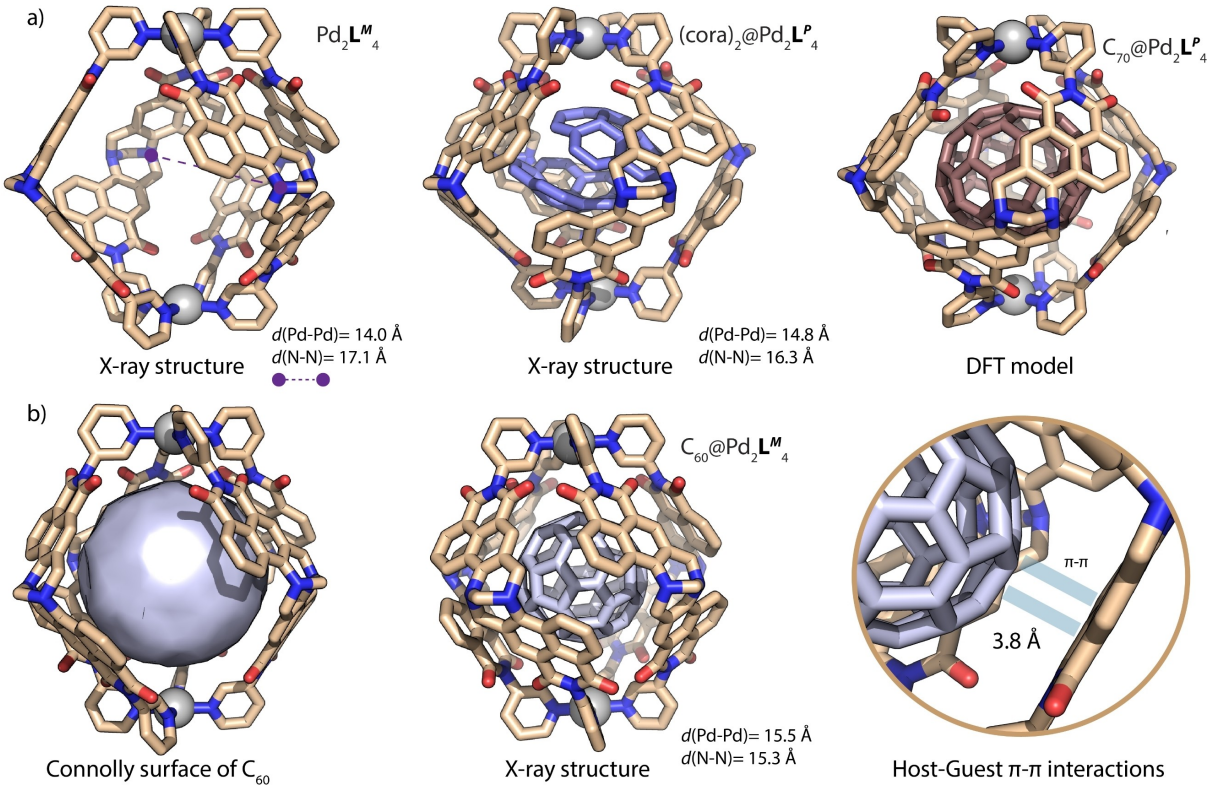

Figure 3. a) From left to right, crystal structures of "empty" $Pd_2\mathbf{L}^{M}_4$, $(cora)_2@Pd_2\mathbf{L}^{P}_4$ and DFT model of $C_{70}@Pd_2\mathbf{L}^{P}_4$. b) Crystal structure of $C_{60}@Pd_2\mathbf{L}^{M}_4$ with the surface representation of the fullerene to highlight the occupied volume of the cavity. The inset shows a zoom on the aromatic panel to C_{60} interaction by π–π stacking. For both a) and b), the Pd–Pd and N–N distances (marked in purple), measured in solid-state, are given to emphasize the "breathing" phenomenon.

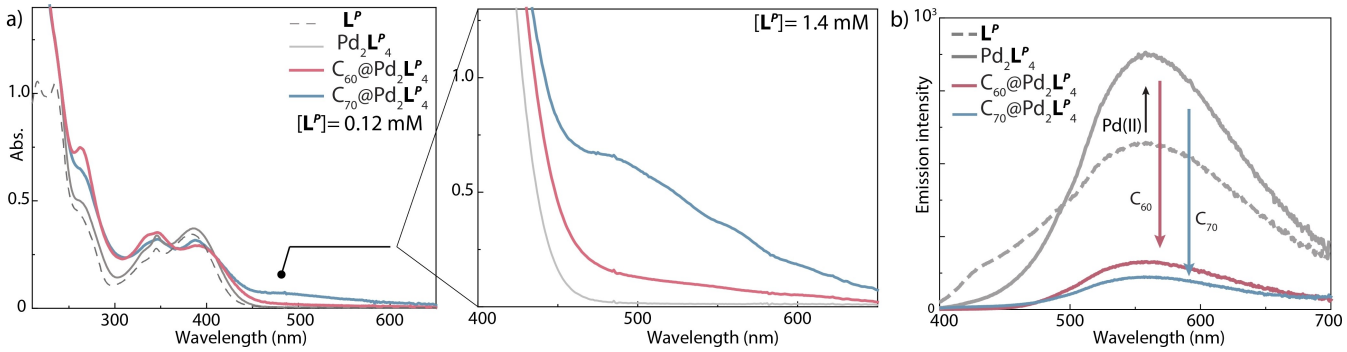

Figure 4. a) The UV/Vis absorption spectra comparison of the ligand, empty cage and the two fullerene host-guest complexes at 0.12 mM in ligand concentration. The right spectrum shows the 450–750 nm region for the same species with a ligand concentration of 1.4 mM. New bands emerging from the symmetry-forbidden $t_{1u}\leftarrow h_u$ electronic transitions of fullerenes C_{60} and C_{70} can be seen. b) The fluorescence emission spectra of the **TBNap** ligand, empty cage and the two fullerene host-guest complexes displaying the luminescence increase upon cage formation and quenching upon guest binding within the cavity.

modifications for the first band at 346 nm, the effect is significantly stronger for the second one. Indeed, not only does the absorption band (initially located at 390 nm) show a clear tailing to higher wavelengths but the emergence of a new band around 500–550 nm becomes observable. Comparison of the UV/Vis absorption spectra at a higher ligand concentration of 1.4 mM, in the assemblies, further strengthens the previous observations. The empty cage absorption band completely disappears at 475 nm (assigned to the ICT) while the one for the cage with C_{60} is extended up to 600 nm. On the other hand, the host-guest complex of C_{70} presents a new band at 485 nm with a shoulder at 565 nm and is still visible at 650 nm at this concentration. The strong π–π interactions between the naphthalimide moieties of the **TBNap** ligands, amplified by the curved shape of the latter, and the fullerenes within the cavity, result in the formation

of an aromatic electron-poor/electron-rich host-guest complex.

Having investigated the ground state interactions, we next measured the fluorescence emission of the **TBNap** ligand $\mathbf{L}^P$ as well as the empty cage $Pd_2\mathbf{L}^P_4$ and the host-guest complex $C_{60}@Pd_2\mathbf{L}^P_4$ (Figure 4b). When excited at 350 nm, $\mathbf{L}^P$ shows a broad emission band centred at 560 nm and tailing up to more than 700 nm, while also displaying a shoulder in the blue region at 430 nm. Interestingly, coordination to Pd(II) led to an increase in the luminescence intensity of the main band and the shoulder disappeared. The emission remained overall broad (400 nm to >700 nm) as is typically observed for such ligands. This increase in emission is likely triggered by a restriction of motion of the ligand in the rather tight cage assembly which results in a suppression of nonradiative pathways. Excitation at higher wavelengths such as 450 nm drastically decreased the intensity of emission and blue-shifted the band to 520 nm. Furthermore, the binding of C_{60} or C_{70} caused a severe quenching in (the **TBNap**) fluorescence of the assembly and the intensity decreased by a factor of five. A conceivable explanation for this phenomenon would be a photoinduced electron transfer (PET) from ligand to fullerene which becomes competitive to the emission pathway (i.e. dark states being populated). This is not surprising, as fullerenes are known to be good electron acceptors.[58,59] Further, DFT calculations (geometry optimization with the ωB97X-D exchange correlation functional (XCF)[60] and def2-SVP basis set[61] and single point energy calculation with the def2-TZVP basis) for both free fullerenes $C_{60/70}$ and the host-guest complexes $C_{60}@Pd_2\mathbf{L}^P_4$ and $C_{70}@Pd_2\mathbf{L}^P_4$ allowed us to obtain and visualize the frontier orbitals of the guests and host-guest species (Figure S69–72). The HOMOs are fully (for the C_{60} complex) or mostly (for the C_{70} complex) located on the ligands while in both cases the LUMOs are located on the fullerene guest.

Quite interesting observations were made when characterizing the homochiral host-guest systems using CD spectroscopy (Figure 5a, see Figure S63 for a plot of g_{abs}). At 0.12 mM concentration of **TBNap** (within the assembly), encapsulation of C_{60} and C_{70} leads to the disappearance of the small Cotton effects at 342 nm, 349 nm and 362 nm, respectively, as well as the change in the CD signal sign at 329 nm. The CD band of the empty cage located at 390 nm is redshifted, especially for C_{70}, reaching 404 nm upon host-guest formation. Eventually, even at this concentration, a new CD band, with very low intensity, can be observed at 530 nm for the C_{70} host-guest complex. Increasing the

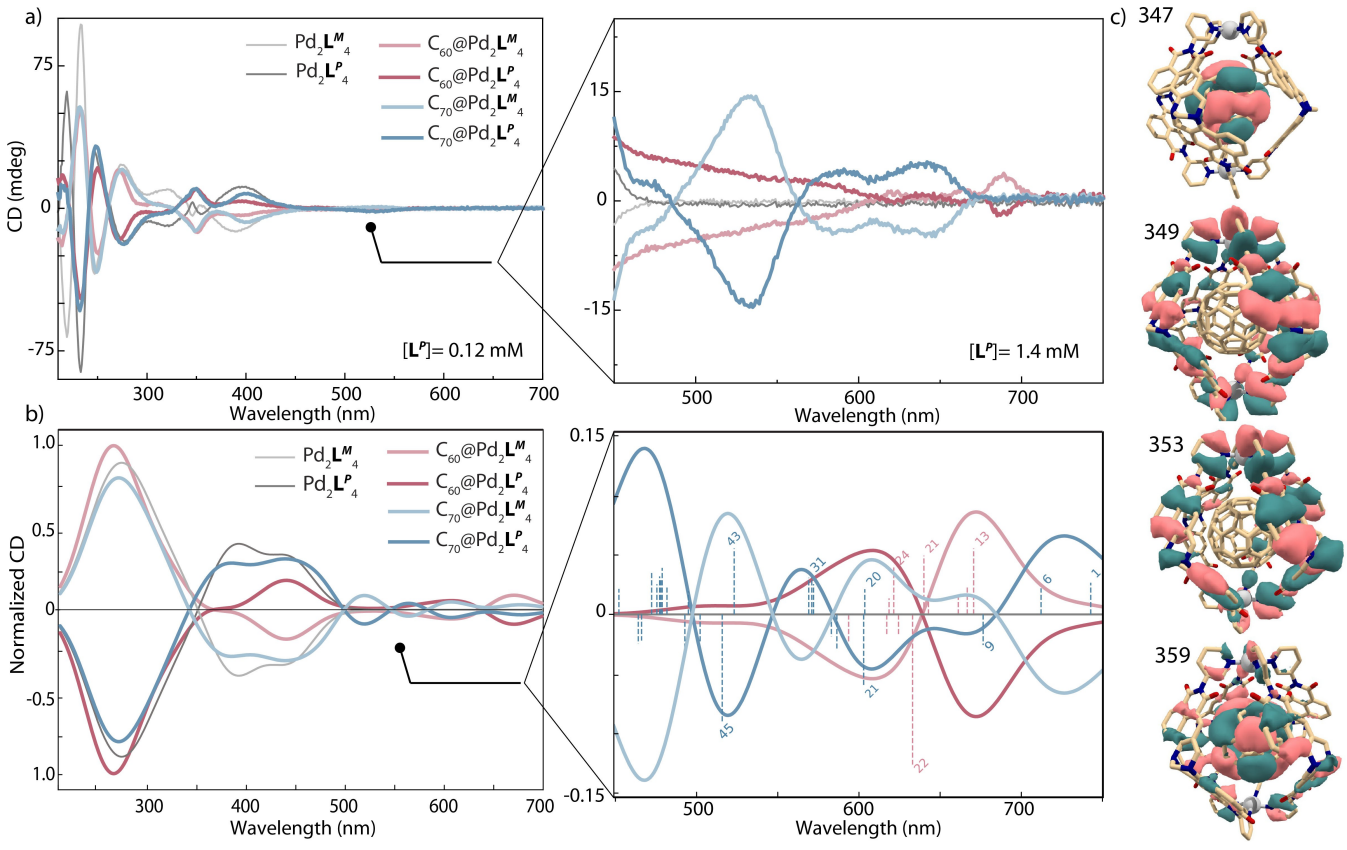

Figure 5. a) CD spectra comparison of the empty cages and the two fullerene host-guest complexes at 0.12 mM in ligand concentration. The right spectrum shows the 450–750 nm region for the same species with a ligand concentration of 1.4 mM. b) Computed CD spectra of the empty cages and the two fullerene host-guest complexes matching experimental data. The numbers on the right spectra correspond to the excited state number yielding major contributions (dashed lines). c) Depiction of the molecular orbitals involved in the dominant CSFs of excited state 13 in the $C_{60}@Pd_2\mathbf{L}^P_4$ complex taken as an example. All MO isosurface pictures were produced using a 0.01 isovalue.

concentration of the **TBNap** ligand to 1.4 mM in the assembly, unambiguously confirmed the appearance of these new CD bands. For the C_{60} host-guest complex, the previously described absorbance tail becomes also observable in the CD ($g_{abs}=2.00\times10^{-3}$ at 500 nm) and small fluctuations are observable after 600 nm with a more pronounced CD band centred at 687 nm ($g_{abs}=1.47\times10^{-3}$). The effect arising from the C_{70} host-guest complex is even more pronounced. Stronger CD bands centred at 530 nm ($g_{abs}=2.18\times10^{-3}$), 590 ($g_{abs}=1.37\times10^{-3}$) as well as 645 ($g_{abs}=3.31\times10^{-3}$) nm were observed. Moreover, a positive Cotton effect at 485 nm is followed by a negative band at 563 nm. All these effects emerge in a region in which neither the free organic ligand nor the empty cage displays any CD absorptions, and therefore can be attributed to the fullerenes' symmetry-forbidden $t_{1u}\leftarrow h_u$ electronic transitions under the influence of the chiral capsule environment.[35,37] This also explains why their intensity is weak as compared to the cage absorptions.

To unambiguously confirm that those absorption and CD bands were the consequence of fullerene-centred transitions, the UV/Vis absorption spectra of C_{60} and C_{70} and the host-guest complexes were recorded in benzene and in a 1:1 acetonitrile/benzene mixture, where all species are soluble (Figure S62). This absorption region (450–700 nm) corresponds to the typical window for symmetry-forbidden $t_{1u}\leftarrow h_u$ transitions in fullerenes (Figure S62). A detailed analysis of the fullerene electronic situation can be found in the experimental section (Figures S71,72). Comparing the spectra of the free and the encapsulated C_{70} or C_{60} (Figure S62) in the previously mentioned absorption region, confirmed their similar origin, as they can be accurately matched. Moreover, these bands are in accordance with those observed in the CD spectra (Figure 5a). Thus, we can assume that the effects observed in the CD experiments are emerging from a host-to-guest chiral induction of the chiral $Pd_2\mathbf{L}^{P/M}{}_4$ capsule onto the pristine fullerene guest within its cavity. We finally proceeded to a control experiment in which free ligand at a concentration of 1.4 mM was mixed with fullerene C_{60} or C_{70} in acetonitrile, sonicated and heated to favour potential fullerene solubilisation (Figure S64). Recording of the CD spectra does not show the previously described bands, underlining the importance of the cage environment both for solubilisation of the fullerene and for the chiral information transfer.

We computed both UV/Vis absorption (see Supporting Information for detailed analysis Figure S74) and the CD spectra (Figure 5b) of the empty host and the two host-guest complexes using the sTDA method,[62,63] def2-TZVP basis set and PBE0 XCF,[63] and could satisfyingly reproduce these spectral features. For all the structures, the strong contribution close to 250 nm was reproduced by the simulations, as was the signal due to the Cotton effect close to 350 nm.

The rich CD feature in the 350–450 nm range also matched well with a broadened tail extending to 450 nm and the weaker signals observed beyond 500 nm. Again, this host-guest binding resulted in major changes in the long-wavelength region, where the empty cage does not present any CD activity.

For $C_{60}@Pd_2\mathbf{L}^{P/M}{}_4$, we observed a slight underestimation of the CD intensity in the 450–550 nm spectral window, while a stronger feature overlapping with the 600 nm tail in the experimental spectrum was correctly modelled. The weaker signals in the 600–650 nm range were more difficult to match by broadening the CD lines with Gaussian distributions, while the stronger features in the 650–700 nm window match well with the simulation (contributions no. 13, 21, and 24 to the $C_{60}@Pd_2\mathbf{L}^{M}{}_4$ signal highlighted with dashed pink lines in Figure 5b). Similar results were obtained for C_{70}. However, the weak tail observed before 500 nm was shown to be more intense in the calculated spectrum. The Cotton effect close to 500 nm and the feature in the 550 nm region were reproduced, while the complex feature in the 550–650 nm range showed an additional Cotton effect slightly below 600 nm, which was not observable in the experiment data. By inspecting the major contributions to the CD spectrum of the $C_{70}@Pd_2\mathbf{L}^{P}{}_4$ complex (dashed blue lines in Figure 5b), the 'dip' in the positive CD band around 600 nm that was observed in the experiment was rationalized by the presence of a strong negative contribution present in the simulation at that wavelength (excited state no. 21). Therefore, the negative band at 600 nm in the predicted CD spectrum was produced primarily because of a major overestimation of such contribution, which shifted the signal to negative values. This discrepancy between the computed spectrum and the observed spectrum then affects the intensity of the signal approximated by Gaussian broadening, while the energy window of the CD signal matches the experiment.

Finally, an analysis of the CIS-like (CIS = configuration interaction singles) wavefunction from the sTDA calculations provided deeper insight into the electronic structure of the host-guest complexes and how the binding affects the resulting optical properties (Table S2, Figure S75). The 400–700 nm window was strongly affected by guest complexation, as signals from the empty cage were negligible. For the sake of brevity, and as an example in Figure 5c, we report the canonical molecular orbitals no. 347, 349, 353, and 359 which are involved in the dominant CSFs (configuration state functions) in excited state number 13 of the $C_{60}@Pd_2\mathbf{L}^{P}{}_4$ complex. Excited state no. 13 shows a strong mixing of the CSFs, which have a large amplitude in the CIS wavefunction. Additionally, the dominant CSFs constitute fullerene-centred excitations and host-guest charge-transfer excitations, where one electron is moved from the fullerene to the naphthalimide walls of the $Pd_2\mathbf{L}^{P}{}_4$ cage. The resonance of these CSFs in the CIS wavefunction results in the spectral features observed in the 400–700 nm regions of the absorption and CD spectra.

Conclusions

We here report a new chiral Pd_2L_4 capsule based on readily accessible, configurationally stable, Tröger's base derived ligands, featuring a cavity that strongly binds fullerenes C_{60} and C_{70} in polar solvents. By embedding the asymmetric moiety right into the backbone of the curved, π-interacting

ligand, a relatively lightweight chiral receptor could be obtained. Through the effect of host-to-guest chiral induction, CD bands arise in the visible region, assigned to characteristic electronic transitions within the fullerene guests. The introduction of chirality to fullerenes has attracted considerable attention over the last years and only a few reports have so far described chirality transfer onto an encapsulated, achiral fullerene via supramolecular interactions.[43] While impressive progress has been made with respect to covalent modification approaches to turn pristine fullerenes into chiral derivatives, this often necessitates laborious synthetic methods and purification effort.[33,64–66] With an emergent interest in the chirality-induced spin selectivity (CISS) effect,[67] growth of research in the field of spintronics,[68,69] and fullerene-based materials,[1,70,71] this type of supramolecular chiral induction promises to find broader application in the near future. Previously, we showed that one can generate a long-lived C_{60} radical anion within the cavity of a Pd_2L_4 capsule based on similar (but achiral) ribbon-shaped ligands.[72] Further studies will now explore the possibility of generating and stabilizing such radical species within the cavity of the herein reported **TBNap** based chiral host to bring organic radicals into a chiral environment. Furthermore, our system is currently studied to serve as a modular platform for the enantioselective covalent derivatization of encapsulated fullerenes.

Supporting Information

The authors have cited additional references within the Supporting Information.[73–83]

Acknowledgements

T. G. and H. M. O'C. thank the Irish Research Council for support (IRC: GOIPD/2020/849), and Dr. Gary Hessman and Brendan Twamley for initial HRMS and X-ray crystallography studies. This work was supported by the Deutsche Forschungsgemeinschaft (DFG) through GRK2376 ("Confinement-Controlled Chemistry", project number 331085229) and under Germany's Excellence Strategy EXC2033, project number 390677874 ("RESOLV"). Diffraction data of $Pd_2\mathbf{L}^{P}_4$, $Pd_2\mathbf{L}^{M}_4$, $C_{60}@Pd_2\mathbf{L}^{M}_4$ and $(cora)_2@Pd_2\mathbf{L}^{P}_4$ was collected at PETRA III and processed on the Maxwell computational resources operated at DESY (Hamburg, Germany) a member of the Helmholtz Association (HGF).[84] We thank Johanna Hakanpää and Helena Taberman for assistance at synchrotron beamline P11 (I-20221120, I-20231259,) and DESY user office for travel funds. Open Access funding enabled and organized by Projekt DEAL.

Conflict of Interest

The authors declare no conflict of interest.

Data Availability Statement

The data that support the findings of this study are available in the supplementary material of this article.

Keywords: coordination cage · chiral induction · fullerene · Tröger's base · circular dichroism

[1] A. M. López, A. Mateo-Alonso, M. Prato, *J. Mater. Chem.* **2010**, *21*, 1305–1318.
[2] J. Liu, L. Qiu, S. Shao, *J. Mater. Chem. C* **2021**, *9*, 16143–16163.
[3] Y. Maeyoshi, A. Saeki, S. Suwa, M. Omichi, H. Marui, A. Asano, S. Tsukuda, M. Sugimoto, A. Kishimura, K. Kataoka, S. Seki, *Sci. Rep.* **2012**, *2*, 600.
[4] E. Castro, A. H. Garcia, G. Zavala, L. Echegoyen, *J. Mater. Chem. B* **2017**, *5*, 6523–6535.
[5] X. Chang, Y. Xu, M. von Delius, *Chem. Soc. Rev.* **2023**, *53*, 47–83.
[6] Y. Xu, S. Gsänger, M. B. Minameyer, I. Imaz, D. Maspoch, O. Shyshov, F. Schwer, X. Ribas, T. Drewello, B. Meyer, M. von Delius, *J. Am. Chem. Soc.* **2019**, *141*, 18500–18507.
[7] J. P. Mora-Fuentes, M. D. Codesal, M. Reale, C. M. Cruz, V. G. Jiménez, A. Sciortino, M. Cannas, F. Messina, V. Blanco, A. G. Campaña, *Angew. Chem. Int. Ed.* **2023**, *62*, e202301356.
[8] J. Song, N. Aratani, H. Shinokubo, A. Osuka, *J. Am. Chem. Soc.* **2010**, *132*, 16356–16357.
[9] D. A. Rothschild, W. P. Kopcha, A. Tran, J. Zhang, M. C. Lipke, *Chem. Sci.* **2022**, *13*, 5325–5332.
[10] L. Wang, G.-T. Wang, X. Zhao, X.-K. Jiang, Z.-T. Li, *J. Org. Chem.* **2011**, *76*, 3531–3535.
[11] A. Sacristán-Martín, D. Miguel, A. Diez-Varga, H. Barbero, C. M. Álvarez, *J. Org. Chem.* **2022**, *87*, 16691–16706.
[12] M. Samanta, A. Rananaware, D. N. Nadimetla, Sk. A. Rahaman, M. Saha, R. W. Jadhav, S. V. Bhosale, S. Bandyopadhyay, *Sci. Rep.* **2019**, *9*, 9670.
[13] A. Saura-Sanmartin, A. Martinez-Cuezva, M. Marin-Luna, D. Bautista, J. Berna, *Angew. Chem. Int. Ed.* **2021**, *60*, 10814–10819.
[14] L. Liu, H. Meng, Y. Chai, X. Chen, J. Xu, X. Liu, W. Liu, D. M. Guldi, Y. Zhu, *Angew. Chem. Int. Ed.* **2023**, *62*, e202217897.
[15] X. Liu, M. Kozlowska, T. Okkali, D. Wagner, T. Higashino, G. Brenner-Weiß, S. M. Marschner, Z. Fu, Q. Zhang, H. Imahori, S. Bräse, W. Wenzel, C. Wöll, L. Heinke, *Angew. Chem. Int. Ed.* **2019**, *58*, 9590–9595.
[16] W. Meng, B. Breiner, K. Rissanen, J. D. Thoburn, J. K. Clegg, J. R. Nitschke, *Angew. Chem. Int. Ed.* **2011**, *50*, 3479–3483.
[17] C. García-Simón, M. Costas, X. Ribas, *Chem. Soc. Rev.* **2015**, *45*, 40–62.
[18] T. Tsutsui, L. Catti, K. Yoza, M. Yoshizawa, *Chem. Sci.* **2020**, *11*, 8145–8150.
[19] M. Moreno-Simoni, T. Torres, G. de la Torre, *Chem. Sci.* **2022**, *13*, 9249–9255.
[20] S. Pullen, J. Tessarolo, G. H. Clever, *Chem. Sci.* **2021**, *12*, 7269–7293.
[21] C. T. McTernan, J. A. Davies, J. R. Nitschke, *Chem. Rev.* **2022**, *122*, 10393–10437.
[22] S. Hasegawa, A. Baksi, B. Chen, G. H. Clever, *Org. Mater.* **2022**, *4*, 222–227.
[23] B. Chen, J. J. Holstein, S. Horiuchi, W. G. Hiller, G. H. Clever, *J. Am. Chem. Soc.* **2019**, *22*, 8907–8913.
[24] C. Colomban, G. Szalóki, M. Allain, L. Gómez, S. Goeb, M. Sallé, M. Costas, X. Ribas, *Chem. Eur. J.* **2017**, *23*, 3016–3022.
[25] N. Kishi, Z. Li, K. Yoza, M. Akita, M. Yoshizawa, *J. Am. Chem. Soc.* **2011**, *133*, 11438–11441.

[26] T. K. Ronson, B. S. Pilgrim, J. R. Nitschke, *J. Am. Chem. Soc.* **2016**, *138*, 10417–10420.
[27] K. Suzuki, K. Takao, S. Sato, M. Fujita, *J. Am. Chem. Soc.* **2010**, *132*, 2544–2545.
[28] D. M. Wood, W. Meng, T. K. Ronson, A. R. Stefankiewicz, J. K. M. Sanders, J. R. Nitschke, *Angew. Chem. Int. Ed.* **2015**, *54*, 3988–3992.
[29] Y. Yang, T. K. Ronson, Z. Lu, J. Zheng, N. Vanthuyne, A. Martinez, J. R. Nitschke, *Nat. Commun.* **2021**, *12*, 4079.
[30] C. García-Simón, M. Garcia-Borràs, L. Gómez, T. Parella, S. Osuna, J. Juanhuix, I. Imaz, D. Maspoch, M. Costas, X. Ribas, *Nat. Commun.* **2014**, *5*, 5557.
[31] E. Ubasart, O. Borodin, C. Fuertes-Espinosa, Y. Xu, C. García-Simón, L. Gómez, J. Juanhuix, F. Gándara, I. Imaz, D. Maspoch, M. von Delius, X. Ribas, *Nat. Chem.* **2021**, *13*, 420–427.
[32] V. Iannace, C. Sabrià, Y. Xu, M. von Delius, I. Imaz, D. Maspoch, F. Feixas, X. Ribas, *J. Am. Chem. Soc.* **2024**, *146*, 5186–5194.
[33] Z. Lu, T. K. Ronson, A. W. Heard, S. Feldmann, N. Vanthuyne, A. Martinez, J. R. Nitschke, *Nat. Chem.* **2023**, *15*, 405–412.
[34] M. Pujals, T. Pèlachs, C. Fuertes-Espinosa, T. Parella, M. Garcia-Borràs, X. Ribas, *Cell Rep. Phys. Sci.* **2022**, *3*, 100992.
[35] G. D. Pantoş, J. Wietor, J. K. M. Sanders, *Angew. Chem. Int. Ed.* **2007**, *46*, 2238–2240.
[36] J. Kou, Q. Wu, D. Cui, Y. Geng, K. Zhang, M. Zhang, H. Zang, X. Wang, Z. Su, C. Sun, *Angew. Chem. Int. Ed.* **2023**, *62*, e202312733.
[37] S. Lo, T. Kitao, Y. Nada, K. Murata, K. Ishii, T. Uemura, *Angew. Chem. Int. Ed.* **2021**, *60*, 17947–17951.
[38] D. B. Straus, R. J. Cava, *Nano Lett.* **2021**, *21*, 4753–4756.
[39] T. Kawauchi, J. Kumaki, A. Kitaura, K. Okoshi, H. Kusanagi, K. Kobayashi, T. Sugai, H. Shinohara, E. Yashima, *Angew. Chem. Int. Ed.* **2008**, *47*, 515–519.
[40] M. Yamashina, T. Tsutsui, Y. Sei, M. Akita, M. Yoshizawa, *Sci. Adv.* **2019**, *5*, eaav3179.
[41] M. Yamashina, S. Kusaba, M. Akita, T. Kikuchi, M. Yoshizawa, *Nat. Commun.* **2018**, *9*, 4227.
[42] M. Yamashina, S. Matsuno, Y. Sei, M. Akita, M. Yoshizawa, *Chem. Eur. J.* **2016**, *22*, 14147–14150.
[43] H. Sasafuchi, M. Ueda, N. Kishida, T. Sawada, S. Suzuki, Y. Imai, M. Yoshizawa, *Chem* **2025**, *11*, DOI: 10.1016/j.chempr.2024.09.031.
[44] B. Chen, J. J. Holstein, A. Platzek, L. Schneider, K. Wu, G. H. Clever, *Chem. Sci.* **2022**, *13*, 1829–1834.
[45] J. M. Delente, D. Umadevi, S. Shanmugaraju, O. Kotova, G. W. Watson, T. Gunnlaugsson, *Chem. Commun.* **2020**, *56*, 2562–2565.
[46] J. I. Lovitt, D. Umadevi, P. R. Lakshmi, B. Twamley, T. Gunnlaugsson, S. Shanmugaraju, *Supramol. Chem.* **2020**, *32*, 620–633.
[47] S. Shanmugaraju, D. Umadevi, L. M. González-Barcia, J. M. Delente, K. Byrne, W. Schmitt, G. W. Watson, T. Gunnlaugsson, *Chem. Commun.* **2019**, *55*, 12140–12143.
[48] U. Kiehne, T. Weilandt, A. Lützen, *Org. Lett.* **2007**, *9*, 1283–1286.
[49] T. Weilandt, U. Kiehne, G. Schnakenburg, A. Lützen, *Chem. Commun.* **2009**, *0*, 2320–2322.
[50] C. Benkhäuser-Schunk, B. Wezisla, K. Urbahn, U. Kiehne, J. Daniels, G. Schnakenburg, F. Neese, A. Lützen, *ChemPlusChem* **2012**, *77*, 396–403.
[51] U. Kiehne, T. Bruhn, G. Schnakenburg, R. Fröhlich, G. Bringmann, A. Lützen, *Chem. Eur. J.* **2008**, *14*, 4246–4255.
[52] U. Kiehne, A. Lützen, *Eur. J. Org. Chem.* **2007**, *2007*, 5703–5711.
[53] T. Weilandt, U. Kiehne, J. Bunzen, G. Schnakenburg, A. Lützen, *Chem. Eur. J.* **2010**, *16*, 2418–2426.
[54] J. B. Maglic, R. Lavendomme, *J. Appl. Crystallogr.* **2022**, *55*, 1033–1044.
[55] B. Mohan, S. Estalayo-Adrián, D. Umadevi, B. la C Poulsen, S. Blasco, G. J. McManus, T. Gunnlaugsson, S. Shanmugaraju, *Inorg. Chem.* **2022**, *61*, 11592–11599.
[56] S.-J. Hu, X.-Q. Guo, L.-P. Zhou, D.-N. Yan, P.-M. Cheng, L.-X. Cai, X.-Z. Li, Q.-F. Sun, *J. Am. Chem. Soc.* **2022**, *144*, 4244–4253.
[57] L. Schoepff, L. Kocher, S. Durot, V. Heitz, *J. Org. Chem.* **2017**, *82*, 5845–5851.
[58] N. S. Sariciftci, L. Smilowitz, A. J. Heeger, F. Wudl, *Science* **1992**, *258*, 1474–1476.
[59] A. J. Stasyuk, O. A. Stasyuk, M. Solà, A. A. Voityuk, *Chem. Eur. J.* **2019**, *25*, 2577–2585.
[60] Y.-S. Lin, G.-D. Li, S.-P. Mao, J.-D. Chai, *J. Chem. Theory Comput.* **2013**, *9*, 263–272.
[61] F. Weigend, R. Ahlrichs, *Phys. Chem. Chem. Phys.* **2005**, *7*, 3297–3305.
[62] S. Grimme, *J. Chem. Phys.* **2013**, *138*, 244104.
[63] C. Adamo, V. Barone, *J. Chem. Phys.* **1999**, *110*, 6158–6170.
[64] W. Shi, Q. Zhuang, R. Zhou, X. Hou, X. Zhao, J. Kong, M. J. Fuchter, *Adv. Energy Mater.* **2023**, *13*, 2300054.
[65] Y. Hashikawa, S. Okamoto, Y. Murata, *Nat. Commun.* **2024**, *15*, 514.
[66] S. Filippone, E. E. Maroto, Á. Martín-Domenech, M. Suarez, N. Martín, *Nat. Chem.* **2009**, *1*, 578–582.
[67] B. P. Bloom, Y. Paltiel, R. Naaman, D. H. Waldeck, *Chem. Rev.* **2024**, *124*, 1950–1991.
[68] S. Ma, J. Ahn, J. Moon, *Adv. Mater.* **2021**, *33*, 2005760.
[69] I. S. Zlobin, Y. V. Nelyubina, V. V. Novikov, *Inorg. Chem.* **2022**, *61*, 12919–12930.
[70] D. M. Guldi, *Chem. Commun.* **2000**, *0*, 321–327.
[71] C.-Z. Li, H.-L. Yip, A. K.-Y. Jen, *J. Mater. Chem.* **2012**, *22*, 4161–4177.
[72] S. Hasegawa, S. L. Meichsner, J. J. Holstein, A. Baksi, M. Kasanmascheff, G. H. Clever, *J. Am. Chem. Soc.* **2021**, *143*, 9718–9723.
[73] Y. Shao, L. F. Molnar, Y. Jung, J. Kussmann, C. Ochsenfeld, S. T. Brown, A. T. B. Gilbert, L. V. Slipchenko, S. V. Levchenko, D. P. O'Neill, R. A. D. Jr, R. C. Lochan, T. Wang, G. J. O. Beran, N. A. Besley, J. M. Herbert, C. Y. Lin, T. V. Voorhis, S. H. Chien, A. Sodt, R. P. Steele, V. A. Rassolov, P. E. Maslen, P. P. Korambath, R. D. Adamson, B. Austin, J. Baker, E. F. C. Byrd, H. Dachsel, R. J. Doerksen, A. Dreuw, B. D. Dunietz, A. D. Dutoi, T. R. Furlani, S. R. Gwaltney, A. Heyden, S. Hirata, C.-P. Hsu, G. Kedziora, R. Z. Khalliulin, P. Klunzinger, A. M. Lee, M. S. Lee, W. Liang, I. Lotan, N. Nair, B. Peters, E. I. Proynov, P. A. Pieniazek, Y. M. Rhee, J. Ritchie, E. Rosta, C. D. Sherrill, A. C. Simmonett, J. E. Subotnik, H. L. W. III. W. Zhang, A. T. Bell, A. K. Chakraborty, D. M. Chipman, F. J. Keil, A. Warshel, W. J. Hehre, H. F. S. III. J. Kong, A. I. Krylov, P. M. W. Gill, M. Head-Gordon, *Phys. Chem. Chem. Phys.* **2006**, *8*, 3172–3191.
[74] J. J. P. Stewart, *J. Mol. Model.* **2007**, *13*, 1173–1213.
[75] F. Weigend, R. Ahlrichs, *Phys. Chem. Chem. Phys.* **2005**, *7*, 3297–3305.
[76] A. Burkhardt, T. Pakendorf, B. Reime, J. Meyer, P. Fischer, N. Stübe, S. Panneerselvam, O. Lorbeer, K. Stachnik, M. Warmer, P. Rödig, D. Göries, A. Meents, *European Phys. J. Plus* **2016**, *131*, 56.
[77] W. Kabsch, *Acta Crystallogr. Sect. D* **2010**, *66*, 133–144.
[78] G. M. Sheldrick, *Acta Crystallogr. Sect. C* **2015**, *71*, 3–8.
[79] C. B. Hübschle, G. M. Sheldrick, B. Dittrich, *J. Appl. Crystallogr.* **2011**, *44*, 1281–1284.

[80] D. Kratzert, J. J. Holstein, I. Krossing, *J. Appl. Crystallogr.* **2015**, *48*, 933–938.
[81] D. Kratzert, I. Krossing, *J. Appl. Crystallogr.* **2018**, *51*, 928–934.
[82] A. L. Spek, *Acta Crystallogr. Sect. C* **2015**, *71*, 9–18.
[83] A. L. Spek, *Acta Crystallogr. Sect. D* **2009**, *65*, 148–155.
[84] Deposition Number(s) 2382045 (for $Pd_2\mathbf{L}^{P}_4$/$Pd_2\mathbf{L}^{M}_4$), 2382046 (for $Pd_2\mathbf{L}^{P}_4$), 2382047 (for $Pd_2\mathbf{L}^{M}_4$), 2382048 (for C_{60}@$Pd_2\mathbf{L}^{M}_4$) and 2382049 (for $(Cor)_2$@$Pd_2\mathbf{L}^{P}_4$) contain the supplementary crystallographic data for this paper. These data are provided free of charge by the joint Cambridge Crystallographic Data Centre and Fachinformationszentrum Karlsruhe Access Structures service.

Manuscript received: October 31, 2024
Accepted manuscript online: December 3, 2024
Version of record online: December 12, 2024